JOURNAL OF NATURAL PRODUCTS

pubs.acs.org/jnp

Article

Structure and Biosynthesis of Desmamides A–C, Lipoglycopeptides from the Endophytic Cyanobacterium *Desmonostoc muscorum* LEGE 12446

Sara Freitas, Raquel Castelo-Branco, Arlette Wenzel-Storjohann, Vitor M. Vasconcelos, Deniz Tasdemir, and Pedro N. Leão*

Cite This: *J. Nat. Prod.* 2022, 85, 1704–1714

Read Online

ACCESS | Metrics & More | Article Recommendations | Supporting Information

ABSTRACT: Certain cyanobacteria of the secondary metabolite-rich order Nostocales can establish permanent symbioses with a large number of cycads, by accumulating in their coralloid roots and shifting their metabolism to dinitrogen fixation. Here, we report the discovery of two new lipoglycopeptides, desmamides A (**1**) and B (**2**), together with their aglycone desmamide C (**3**), from the nostocalean cyanobacterium *Desmonostoc muscorum* LEGE 12446 isolated from a cycad (*Cycas revoluta*) coralloid root. The chemical structures of the compounds were elucidated using a combination of 1D and 2D NMR spectroscopy and mass spectrometry. The desmamides are decapeptides featuring *O*-glycosylation of tyrosine (in **1** and **2**) and an unusual 3,5-dihydroxy-2-methyldecanoic acid residue. The biosynthesis of the desmamides was studied by substrate incubation experiments and bioinformatics. We describe herein the *dsm* biosynthetic gene cluster and propose it to be associated with desmamide production. The discovery of this class of very abundant (>1.5% d.w.) bacterial lipoglycopeptides paves the way for exploration of their potential role in root endosymbiosis.

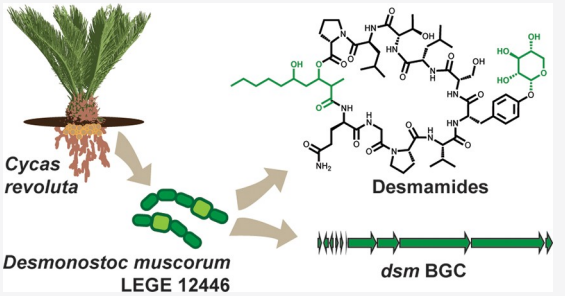

Cyanobacteria are photoautotrophic bacteria found in a wide range of environments and exist in single-celled, colonial, filamentous, and branched filamentous forms.[1] These organisms can also differentiate into specialized cells,[1] such as heterocysts, which carry out nitrogen fixation[2] and are the hallmark of the Nostocales, a late-branching order within the Cyanobacteria phylum. Nostocalean cyanobacteria typically have large genomes and complex morphological features and can be either free-living, obligate symbionts of the water fern *Azolla* or facultative symbionts of other organisms, such as cycads, mosses, liverworts, and fungi.[1,3] In cycads, the cyanobacterial holobiont forms a conspicuous circular layer in the coralloid roots.[4] Free-living cyanobacterial holobionts are recruited by the plant and can invade their host at different stages of root development.[3,4] Once inside the roots, the cyanobacteria increase their heterocyst differentiation frequency to fix nitrogen for the host and establish a permanent symbiosis under complete darkness.[3,4] Cyanobacteria within the order Nostocales present relatively large genomes (average 7.6 Gb),[5] which typically contain between 10 and 30 biosynthetic gene clusters (BGCs), encoding the production of several classes of natural products.[6] These include terpenes, alkaloids, peptides of ribosomal (RiPPs) or nonribosomal (NRPs) origin, polyketides, and hybrids thereof.[6,7] The chemical talent of members of the Nostocales was well-recognized before the genomic era: early discoveries of natural products from this order include remarkable structures such as the cylindrocyclophanes,[8] hapalindoles and related alkaloids,[9] cryptophycins,[10] and scytonemin.[11] Symbiotic Nostocales are known to be rich producers of secondary metabolites,[12,13] some of which have been shown to mediate interactions with the host.[14,15] For example, the facultative cycad symbiont cyanobacterium *Nostoc punctiforme* PCC 73102 produces the nostopeptolides, cyclic lipopeptides whose production is regulated by the plant host and are involved in cross-talk between the two organisms.[15] A large variety of cyanobacteria and, in particular, members of the order Nostocales produce cyclic lipopeptides.[16] These compounds are usually synthesized by hybrid polyketide synthase/nonribosomal peptide synthetase (PKS/NRPS) pathways, which yields a fatty acyl moiety (that can be modified to varying degrees) connected to a peptidic component.[16] Cyanobacterial cyclic lipopeptides are structurally diverse and typically exhibit antifungal activity; however their precise ecological roles are mostly unknown.[16]

A very small fraction of natural cyclic lipopeptides—from cyanobacteria or other organisms—are glycosylated and

Received: February 16, 2022
Published: July 6, 2022

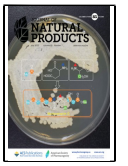

https://doi.org/10.1021/acs.jnatprod.2c00162
J. Nat. Prod. 2022, 85, 1704–1714

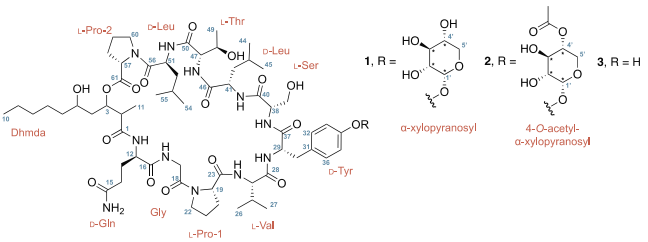

referred to as lipoglycopeptides. This designation has been used to encompass both glycosylated lipopeptides and acylated glycopeptides.[17,18] Natural lipoglycopeptides are rare and are grouped in a small number of structural classes: the cyanobacterial hassallidins/balticidins,[19,20] the actinobacterial teicoplanin/teichomycins,[21] mannopeptimycins (γ, δ, and ε),[22] ramoplanins,[23] and gausemycins,[18] as well as occidiofungins produced by a Gram-negative *Burkholderia* strain.[24] Potent antibacterial or antifungal activities are associated with each of these compound classes; teicoplanin and related semisynthetic lipoglycopeptides are used in the clinic to treat serious infections caused by Gram-positive bacteria.[25]

In this study, we report the chemical exploration of the nostocalean cyanobacterium *Desmonostoc muscorum* LEGE 12446, a plant facultative symbiont isolated from a cycad (*Cycas revoluta*) coralloid root. Metabolomic analysis of a prefractionated organic extract of this cyanobacterium led to the detection and eventual isolation of two abundant metabolites, desmamides A (**1**) and B (**2**), which represent a new structural class of lipoglycopeptides. Their aglycone, desmamide C (**3**), was also isolated in this effort. The biosynthesis of **1**−**3** was investigated, and a putative BGC associated with desmamide production (*dsm*) was identified. Compound **2** inhibited the growth of the plant pathogenic bacterium *Xanthomonas campestris* with moderate potency.

RESULTS AND DISCUSSION

MS-Guided Isolation of Desmamides A−C (1−3). As part of our ongoing investigations of the chemical diversity of cyanobacteria from the LEGE culture collection (LEGEcc),[26] we carried out an exploration of a xenic, unicyanobacterial culture of *D. muscorum* LEGE 12446. The biomass from a small-scale laboratory culture of *D. muscorum* was extracted with CH_2Cl_2/MeOH (2:1, v/v) and fractionated in an SPE column. Global Natural Products Social Molecular Networking (GNPS)[27] analysis of the resulting fractions revealed the presence of a cluster comprising five mass features in the fraction eluting with 100% MeOH, two of which had close retention time values and $[M + H]^+$ ions with m/z 1388.750, and 1256.714 (Figure S1; Table S1). Dereplication using the GNPS tools Dereplicator,[28] Dereplicator VarQuest,[29] and Dereplicator+[30] as well as manual searches on the Dictionary of Natural Products database[31] and Natural Products Atlas[32] returned no hits, confirming the novelty of the compounds. To obtain sufficient amounts of the natural products for NMR-based structure elucidation and biological activity testing, the strain was grown in large scale (160 L), which yielded 70.3 g of dry biomass. Repeated percolation with CH_2Cl_2/MeOH (2:1, v/v) afforded an organic extract (14.7 g) that contained the target mass features, as revealed by liquid chromatography coupled to high-resolution electrospray ionization mass spectrometry (LC-HRESIMS) analysis, enabling an MS-guided isolation approach (Figure S2). To this end, we performed a normal-phase vacuum liquid chromatography (VLC) of the organic extract to obtain 13 fractions of increasing polarity. LC-HRESIMS analysis indicated that the compounds were abundant in fractions eluting with 1:2 and 3:7 EtOAc/MeOH (v/v). These fractions were combined (2.90 g), and LC-HRESIMS analysis was used to follow the targeted mass features over a series of chromatographic procedures. Normal-phase flash chromatography, reversed-phase chromatography on a prepacked SPE cartridge, and semipreparative and analytical HPLC were necessary to obtain pure desmamides A (**1**, 26.3 mg) and B (**2**, 20.4 mg), together with their aglycone, desmamide C (**3**, 4.0 mg). Compounds **1** and **3** correspond to the two GNPS-detected mass features targeted, while compound **2** was obtained during isolation of **1**. A considerable amount of **1**−**3** remained in adjacent chromatography fractions; we estimate, based on LC-HRESIMS quantification (Figure S3, Table S2), that the combined mass of these metabolites reaches 235 mg in the initial extract (1.6% of dry cell material).

Structure Elucidation of 1−3. We focused our structure elucidation efforts on the most abundant metabolite, **1**. HRESIMS analysis of **1** showed an m/z 1388.7577 for the $[M + H]^+$ ion (Figure S4). This was consistent with a molecular formula of $C_{66}H_{105}N_{11}O_{21}$ and the presence of 20 degrees of unsaturation. Inspection of the ^1H and ^{13}C APT NMR data (400 MHz, DMSO-d_6) of **1** (Table 1) quickly revealed the presence of the anomeric proton (H-1′, δ_C 97.6, δ_H 5.31 $J_{1'-2'}$ 3.5 Hz) of a sugar unit. Multiple resonances consistent with the exchangeable NH protons (δ_H 8.5−7.50), amide carbons (δ_C 175−165), and alpha positions of amino acid residues (δ_C 60−40, δ_H 4.5−3.5) were observed (Table 1). Furthermore, an aliphatic terminal methyl group triplet (CH_3-10, δ_C 14.0, δ_H 0.86) and a small methylene envelope (δ_H 1.28−1.25) were clearly identified (Table 1). These observations collectively suggested that **1** was a lipoglycopeptide. Combined analysis of 1D and 2D (HSQC, HMBC, and COSY) NMR data for **1** (Table 1, Figure 1) indicated that a major conformer and at least one minor conformer existed in solution, complicating the interpretation of the NMR spectra. Still, our analysis enabled the assembly of several structural fragments (Figure 1A), including those of a number of proteinogenic amino acid residues (Thr, Ser, Gln, two Pro, Val, Gly, and two Leu). Furthermore, it was possible to establish the presence of a Tyr residue featuring *O*-glycosylation with an aldopentose pyranose ring, as the anomeric proton showed an HMBC correlation to C-34 and NOE correlation to H-33/35. Determination of the nature of the sugar residue connected to Tyr in **1** was hampered by extensive overlap of the sugar proton multiplet signals, limiting our ability to measure the associated coupling constants. Still, the clear $J_{1'-2'}$ value of 3.5 Hz for the anomeric proton (H-1′) indicated α-glycosylation. To identify the chemical nature of the sugar unit in **1**, we carried out an acid hydrolysis to free the sugar unit, followed by LC-HRESIMS analysis of 1-phenyl-3-methyl-5-pyrazolone (PMP) derivatives of ribose, xylose, and arabinose and of the hydrolyzed sugar residue of **1**. Interestingly, this analysis indicated that xylose was the most abundant sugar in **1** (~80%), but arabinose was also found to a smaller extent (~20%, from LC-HRESIMS, Figure S12). Hence, it is possible that some of the predicted minor conformer resonances observed in the NMR data for **1** could actually correspond to this arabinose-bearing, coeluting minor compound. The presence of an α-methylated and β- and δ-hydroxylated acyl moiety could also be deduced from the NMR data. This spin

https://doi.org/10.1021/acs.jnatprod.2c00162
J. Nat. Prod. 2022, 85, 1704−1714

Table 1. ^{1}H (400 MHz) and ^{13}C (100 MHz) NMR Spectroscopic Data for Desmamide A (1) in DMSO-d_6

unit	no.	δ_C, type	δ_H[a] (J in Hz)	HMBC[b]	COSY	NOESY
Dhmda	1	172.5, C				
	2	43.7, CH	2.55, t (6.7)	1, 3, 4, 11	3, 11	4, Gln-NHa
	3	72.9, CH	5.06, m	1, 2, 4, 5, 11, 61	2, 4	11, Gln-NHa
	4	38.4, CH_2	1.46, m	3, 5	3, 5	2, Gln-NHa
	5	66.3, CH	3.33, m	7	4, 6, Dhmda-OH	
	6	37.7, CH_2	1.28, m	7	5	
	7	24.8, CH_2	1.28, m	6, 8		
	8	24.8, CH_2	1.28, m	6, 8, 9		
	9	22.1, CH_2	1.25, m	6, 8, 10	10	
	10	14.0, CH_3	0.86, m	9	9	
	11	13.6, CH_3	0.98, d (7.0)	1, 2, 3	2	3, Gln-NHa
	OH		4.30, d (5.7)	4, 5, 6	5	
Gln	12	53.1, CH	4.15, m	1, 13, 14, 16	13a, 13b, Gln-NHa	Gly-NH
	13a	27.7, CH_2	1.86, m	12, 14, 15	12	Gln-NHa
	13b		1.74, m	12, 14, 15	12, 14a	Gln-NHa
	14a	31.7, CH_2	2.12, m	12, 13, 15	13b	Gln-NHa
	14b		1.88, m	12, 15		Gln-NHa
	15	173.8, C				
	16	171.7, C				
	NHa		7.93, m	1, 12	12	2, 3, 4, 11, 13a, 13b, 14a, 14b
	NHb		6.72, d (11.5)	14, 15	Gln-NHb	
	NHb		7.20, d (18.8)	15	Gln-NHb	
Gly	17a	41.3, CH_2	3.96, m	16, 18	17b, Gly-NH	
	17b		3.80, m	16, 18	17a	Gly-NH
	18	167.1, C				
	NH		7.76, t (5.3)	16	17a	12, 17b
Pro_1	19	59.2, CH	4.38, m	21, 23	20	Val-NH
	20	28.9, CH_2	2.0, m	21, 22, 23	19	
	21	24.4, CH_2	1.97, m		22a	22b
	22a	46.6, CH_2	3.51, m		21, 22b	
	22b		3.75, m		22a	21
	23	172.4, C				
Val	24	59.8, CH	3.76, m	25, 27, 28	25, Val-NH	26, Tyr-NH
	25	29.5, CH	1.72, m	24, 26, 27, 28	24, 26, 27	Val-NH
	26	18.6, CH_3	0.46, d (6.6)	24, 25, 27	25	24, Val-NH
	27	18.7, CH_3	0.66, d (6.6)	24, 25, 26	25	Val-NH
	28	170.4, C				
	NH		8.11, d (5.8)		24	19, 25, 26, 27
Tyr	29	54.1, CH	4.53, m	28, 30, 37	30a, 30b, Tyr-NH	32/36, Tyr-NH, Ser-NH
	30a	36.6, CH_2	2.64, m	32/36, 29	29, 30b	32/36, Tyr-NH
	30b		3.13, m	32/36	29, 30a	32/36, Tyr-NH
	31	131.2, C				
	32	129.9, CH	7.13, d (8.5)	30, 33, 34	33/35	29, 30a, 30b
	33	116.5, CH	6.91, d (8.5)	31, 34	32/36	1′
	34	155.4, C				
	35	116.5, CH	6.91, d (8.5)	30, 33, 34	32/36	1′
	36	129.9, CH	7.13, d (8.5)	31, 34	33/35	29, 30a, 30b
	37	171.5, C				
	NH		8.21, d (8.4)	28	29	24, 29, 30a, 30b
Ser	38	56.5, CH	4.16, m	37, 39, 40	Ser-NH	39a
	39a	61.5, CH_2	3.65, m	40	Ser-OH	38, Ser-NH
	39b		3.75, m	40	Ser-OH	
	40	169.8, C				
	NH		8.08, d (6.8)	37, 38, 39	38	29, 39a, Ser-OH, Leu_1-NH
	OH		5.13, t (6.1)	39	39a, 39b	Ser-NH
Leu_1	41	48.8, CH	4.32, m		Leu_1-NH	42, Leu_1-NH
	42	40.3, CH_2	1.42−1.50, m	41, 43, 44/45		41, Leu_1-NH
	43	24.0, CH	1.64, m	42, 44/45	44/45	
	44	23.2, CH_3	0.87, m	43	43	
	45	23.2, CH_3	0.87, m	43	43	
	46	172.1, C				

https://doi.org/10.1021/acs.jnatprod.2c00162
J. Nat. Prod. 2022, 85, 1704−1714

Table 1. continued

unit	no.	δ_C, type	δ_H[a] (J in Hz)	HMBC[b]	COSY	NOESY
	NH		7.55, d (8.0)	40	41	41, 42, Ser-NH, Thr-NH
Thr	47	58.3, CH	4.19, m	46, 48, 49, 50	Thr-NH	48, 49
	48	66.8, CH	3.91, m	50	49, Thr-OH	47, Thr-NH, Leu_2-NH
	49	19.4, CH_3	1.0, d (6.4)	47, 48	48	47, Thr-OH
	50	169.5, C				
	NH		7.87, d (7.5)	46, 47, 48	47	48, Leu_1-NH, Thr-OH
	OH		4.90, d (4.6)	47, 48, 49	48	49, Thr-NH
Leu_2	51	48.8, CH	4.65, m	50, 56	52, Leu_2-NH	
	52	41.1, CH_2	1.48, m	51, 53, 54/55	51	Leu_2-NH
	53	24.0, CH	1.64, m	52, 54/55	54/55	
	54	21.4, CH_3	0.83, m	52, 53	53	
	55	21.4, CH_3	0.83, m	52, 53	53	
	56	170.6, C				
	NH		7.57, d (8.0)	50	51	48, 52
Pro_2	57	59.0, CH	4.27, dd (3.5, 8.7)	58, 59, 61	58	59, 3′
	58	28.5, CH_2	2.13, m		57, 59	
	59	24.7, CH_2	1.85, m	58, 60	58, 60	57
	60	45.9, CH_2	3.46, m		59	
	61	171.4, C				
xylosyl	1′	97.6, CH	5.31, d (3.5)	34, 63, 64, 66	2′	33/35
	2′	71.6, CH	3.36, m	64, 66	1′, OHa	
	3′	73.2, CH	3.55, m	63, 65	OHb	57
	4′	69.7, CH	3.34, m	64, 66		
	5′a	62.5, CH_2	3.45, m	62, 64, 65	5′b	
	5′b		3.33, m	62	5′a	OHb, OHc
	OHa		5.01, d (6.2)		2′	
	OHb		4.93, d (4.9)	63, 64, 65	3′	5′b
	OHc		4.99, d (4.8)	65, 66		5′b

[a]From HSQC. [b]From proton to indicated carbon.

system was supported by HMBC and COSY correlations (Figure 1A) and degenerated into aliphatic methylenes, which could be connected by HMBC correlations to a terminal linear alkane moiety (Figure 1A). Hence, this residue was found to correspond to a 3,5-dihydroxy-2-methyldecanoic acid (Dhmda) residue, *O*-substituted at C-3 (Figure 1A). Due to poor resolution of the multiple amide carbon resonances, inter-residue connectivity could not be unambiguously established from the initial HMBC data acquired for **1**. To circumvent this, we resorted to a band-selective constant-time HMBC[33] experiment (Figure S11). The increased resolution in the amide δ_C resonance region enabled the determination of the connectivity between the NMR-derived residues for **1**, with the exception of the (Pro-1)−Val connectivity (Figure 1A). Nevertheless, a cyclic peptide would be required to satisfy the degrees of unsaturation, and the connectivity between Pro and Val was supported by NOE data (Figure 1A). From HRESIMS/MS analysis of **1**, the residue sequences [Dhmda-Gln-Gly-Pro-Val-Tyr] and [Tyr-Ser-Leu-Thr-Leu-Pro-Dhmda-Gln] could be established (Figures 1A, S13, S14), which validated the NMR-derived findings.

The 1D and 2D NMR data of **2** in DMSO-d_6 (Table S3) were found to be highly similar to those of **1**. In HRESIMS analysis, **2** showed an m/z 1430.7666 corresponding to a molecular formula $C_{68}H_{108}N_{11}O_{22}$ and 21 degrees of unsaturation. The 42.0089 amu mass difference from **1** is consistent with the presence of an acetyl substitution (C_2H_2O, calcd 42.0106 amu). Comparison of the ^1H and ^{13}C NMR data of **1** and **2** revealed the differences to be associated with the sugar resonances, including those of C-3′/4′/5′ (Table S3). Also, a prominent sharp singlet (δ_H 2.02, s, 3H) and an additional carbonyl resonance (δ_C 170.0) were observed in **2**. Analysis of 2D NMR data of this compound (Table S3) clarified that the latter signals corresponded to the suspected acetyl group, in particular through the ^2J HMBC correlation between the acetyl methyl to the carbonyl (Figure 1B). An HMBC correlation between H-4′ and this same carbonyl confirmed the acetylation of the OH group at the C-4′ position of the sugar moiety (Figure 1B). The acetylated sugar residue is proposed to be α-xylopyranosyl, as in **1**, on the basis of the small $J_{1'\text{-}2'}$ value of 3.5 Hz (H-1′, δ_H 5.40) and from coupling constant analysis of ^1H and COSY data (Table S3).

Compound **3** showed ^1H and ^{13}C NMR data in DMSO-d_6 (Table S4) similar to those of **1** and **2** but lacking the sugar signals, while featuring a broad singlet resonating at δ_H 9.13, characteristic of a phenol group exchangeable proton. As suggested by the NMR data, this metabolite was confirmed to be the aglycone of **1** and **2** on the basis of identical HRESIMS/MS spectra for **3** and the in-source isolated aglycone ions of **1** and **2** (Figures 1C, S23).

The absolute configurations of the chiral amino acid residues in **1** (and therefore also in **2** and **3**) were determined using chiral-phase HPLC and Marfey's analysis. The Tyr residue, Gln residue, and the two Leu residues were found to have the D-configuration, while the remaining chiral amino acids were of L-configuration (Figures S24, S25). We were unable to determine the absolute configuration of the α-xylopyranosyl residue and thus report only relative configuration. Nevertheless, given the fact that L-xylose is very rare in nature,[34] we propose a D-configuration for this sugar residue.

https://doi.org/10.1021/acs.jnatprod.2c00162
J. Nat. Prod. 2022, 85, 1704−1714

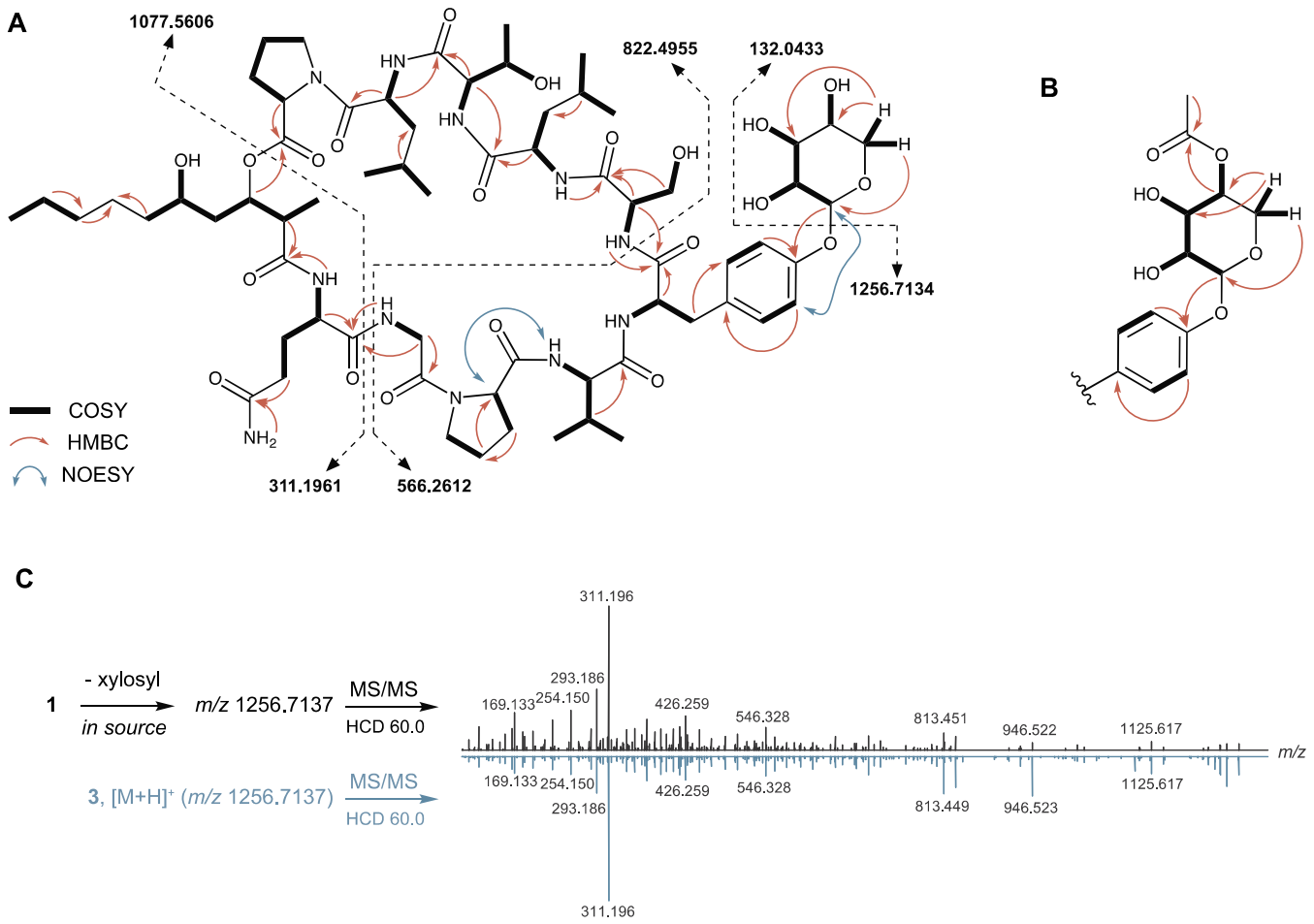

Figure 1. Structure elucidation of **1**−**3**. (A) Key HMBC, COSY, and NOESY correlations and HRMS/MS fragmentations supporting the structure proposal for **1**. (B) Key HMBC and COSY correlations supporting the presence of a 4-*O*-acetylxylopyranosyl-Tyr moiety. (C) Comparison of the HRESIMS/MS spectra of the aglycone of **1** (isolated in-source) and of compound **3**, supporting that they are identical.

Compounds **1** and **2** are cyclic decapeptides that feature Tyr *O*-glycosylation and contain a modified fatty acyl residue as part of the macrocycle. This residue is connected through an amide bond to the N-terminal amino acid and through an ester bond to the C-terminus of the peptide chain. Desmamides A and B thus represent a novel lipoglycopeptide class, the second to be described in cyanobacteria after the hassallidins/balticidins.[19,20] Unlike **1** and **2**, these compounds are nonapeptides with an exocyclic fatty acyl residue connected to the N-terminal amino acid, which is also exocyclic. Several *O*-glycosylation patterns have been described for hassallidins/balticidins, occurring on the 3-hydroxy group of the fatty acyl moiety and/or on the endocyclic N-Me-Thr residue. Compounds **1** and **2** are also structurally distinct from the other previously reported natural lipoglycopeptide scaffolds (Figure S26). Nevertheless and remarkably, *O*-glycosylation of Tyr is observed in several of these, namely, in mannopeptimycins $\gamma/\delta/\varepsilon$[22] and in the gausemycins.[18] This decoration is also present in the fungal glycopeptide cycloaspeptide F[35] and in cacaoidin,[36] a recently described ribosomally synthesized and post-translationally modified (RiPP) glycopeptide. In the case of ramoplanin, *O*-glycosylation occurs in the non-proteinogenic amino acid Hpg (4-hydroxyphenylglycine),[23] which is structurally similar to Tyr. Protection of the 4-OH position in sugar residues, as observed for **2**, is also a feature of mannopeptimycins $\gamma/\delta/\varepsilon$,[22] while several hassallidins contain acetylated sugar moieties.[20] We could not find other examples of lipopeptides bearing a Dhmda moiety nor shorter- or longer-chain versions thereof.

Identification and Analysis of the *dsm* Biosynthetic Gene Cluster. We next looked into the biosynthesis of the desmamides. The structures of **1**−**3** could, in principle, be reconciled with canonical, hybrid PKS and NRPS biosynthetic logic. This working hypothesis was used to search the genome data of *D. muscorum* LEGE 12446 (GenBank: JADEXS020000000). Annotation of the genome data using antiSMASH v6.0[37] revealed several hybrid PKS-NRPS BGCs. One such BGC featured two PKS modules upstream of 10 NRPS modules, for which the corresponding adenylation (A) domains are predicted to select and activate the amino acids that make up the desmamides (Figure 2A). Notably, these are collinear with the N-to-C terminal amino acid sequence of the peptide and contained epimerase (E) domains in the modules predicted to load the experimentally determined D-amino acids. We considered this BGC further as the putative desmamide gene cluster (*dsm*) and carried out a detailed annotation (Figure 2A, Table S5), which led us to generate a biosynthetic proposal (Figure 2B). According to our proposal, the biosynthesis of **1**−**3** begins with activation of hexanoic acid by an adenylation domain in DsmG, which is related to fatty acyl-AMP ligases (Table S5). This intermediate would then be elongated using malonyl-CoA by the PKS module in DsmG,

https://doi.org/10.1021/acs.jnatprod.2c00162
J. Nat. Prod. 2022, 85, 1704−1714

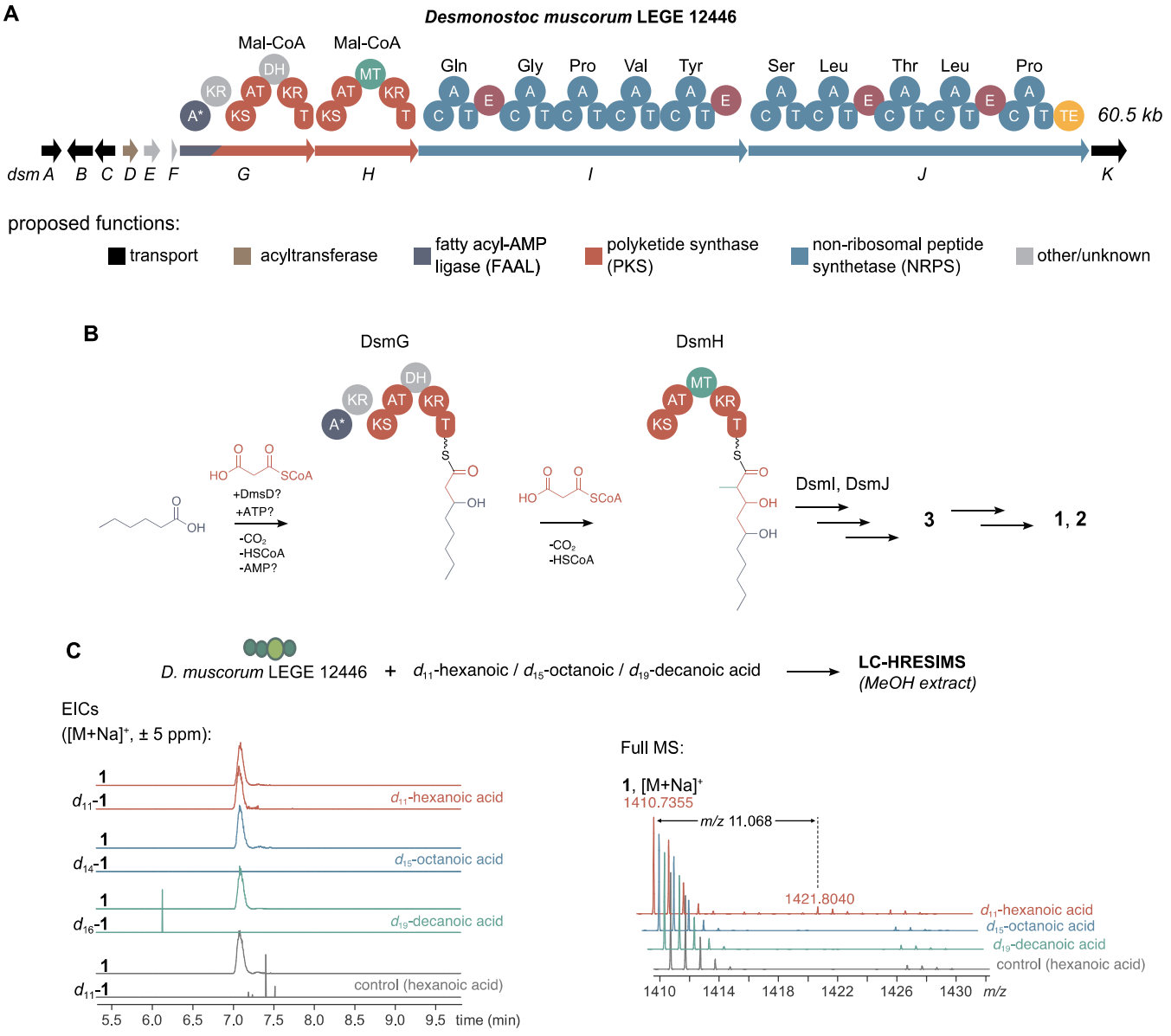

Figure 2. Biosynthesis of the desmamides A–C (**1**–**3**). (A) Schematic representation of the *dsm* BGC, including the proposed functions of the predicted open-reading frames, domain composition of detected PKS and NRPS (or NRPS-like) modules, and bioinformatically predicted (antiSMASH) monomers activated by acyl-tranferase (AT) or adenylation (A) domains. A* indicates an adenylation domain within a region with homology to a fatty acyl-AMP ligase (FAAL), proposed to activate hexanoic acid. (B) Proposed biosynthetic steps leading to **1**–**3**, highlighting the formation of the Dhmda residue from hexanoic acid, by PKS machinery. (C) LC-HRESIMS analysis of methanolic extracts of *D. muscorum* LEGE 12446 cultures supplemented with perdeuterated fatty acids. Shown are EICs for *m*/*z* values corresponding to $[M + H]^+$ ions for compound **1** and for hypothesized isotopologues resulting from incorporation of each of the perdeuterated fatty acids. Also shown is full MS data, highlighting the mass shift supporting incorporation of d_{11}-C_6 into **1**.

which includes a ketoreductase domain (KR), to generate a linear eight-carbon beta-hydroxy acyl-ACP intermediate. An additional malonyl-CoA unit would then be used by the PKS module in DsmH to elongate this intermediate to a 10-carbon unit, reduce its beta-keto group (KR domain), and methylate (methyltransferase domain, MT) its α position to generate the 11-carbon Dhmda residue. In both PKS modules, the KR domains do not present residue signatures that enable inferring the configuration of C-2, C-3, and C-5, as evidenced by antiSMASH v6.0 analysis, which did not result in a classification of the KR type for either domain. To test the proposed biosynthesis of Dhmda experimentally, in particular whether hexanoic acid (C_6) is the starter unit for the biosynthesis of **1**–**3**, we supplemented *D. muscorum* LEGE 12446 cultures with perdeuterated fatty acids, namely, hexanoic (d_{11}-C_6), octanoic (d_{15}-C_8), and decanoic (d_{19}-C_{10}) acids. LC-HRESIMS analysis showed that only d_{11}-C_6 was incorporated into **1**–**3** (Figure 2C), indicating that hexanoic acid is a substrate in the biosynthesis of the desmamides, as hypothesized. However, we could not find any ACP domain in between the adenylation domain proposed to load hexanoic acid and the first PKS module, which is unusual. A KR domain downstream of the A domain in DsmG is of the C-1 type and therefore inactive.[38] The PKS module of DsmG includes a DH domain, containing all catalytic residues (as per antiSMASH analysis), which does not seem necessary to generate the

https://doi.org/10.1021/acs.jnatprod.2c00162
J. Nat. Prod. 2022, 85, 1704−1714

Dhmda residue of **1**−**3**. As per our proposal and canonical hybrid PKS/NRPS biosynthesis,[39] the resulting C_{11} acyl intermediate is passed to the first NRPS module in DsmI, which loads Gln, followed by incorporation of the additional amino acids into the growing chain by the NRPS machinery encoded in DsmI and DsmJ. Finally, the thioesterase in the C-terminus of DsmJ would catalyze the concomitant cyclization and chain release of the desmamides (Figure 2A,B).

Intriguingly, despite **1** and **2** being glycosylated, we could not find a glycosyltransferase-encoding gene in the *dsm* locus or its genomic neighborhood. A genome-wide search for GTs, in particular those known to glycosylate tyrosine residues in the biosynthesis of natural products, indicated multiple GTs, some of which were low-identity homologues of the cacaoidin BGC GTs (Table S6); however none were near the *dsm* locus. Homologues of the mannopeptimycin glycosyltransferases[40] were not detected in our searches. It is also unclear if any of the *dsm* BGC-encoded enzymes are responsible for the 4-*O*-acetylation of the sugar residue. One possibility would be the predicted acyltransferase DsmD. Enzymes containing a GNAT-like fold such as DsmD (which contains two GNAT-like domains) are known to *N*-acylate several substrates[41] but have also been reported to catalyze *O*-acetylation of sugar residues.[42,43] Interestingly, hassallidins also feature *O*-acetylation in sugar residues decorating the peptide. In this case, the authors suggested that HasR, an acyltransferase encoded in the hassallidin (*has*) BGC, could be responsible for these decorations.[20] We were unable to detect any homologues of HasR in the genome of *D. muscorum* LEGE 12446.

Hassallidins are widely distributed among the Nostocales.[20] We wondered if this was the case for desmamides and whether *dsm*-like BGCs could be found in genomes of cultured cyanobacteria or in metagenome data. The ClusterBlast tool in antiSMASH could not retrieve any similar BGCs, and BlastP searches (nr/env_nr databases) using DsmG/DsmH/DsmI/DsmJ amino acid sequences as query did not retrieve hits with a genomic context that would configure a full *dsm* BGC. Curiously, several Dsm proteins have a very high identity to homologues from *Nostoc* sp. FACHB-973 and *Desmonostoc muscorum* CCALA 125 (Table S5). Because such homologues are present in more than one contig in each of the genome assemblies, it is unclear if these are part of *dsm* BGCs.

Biological Activities. Compounds **1** and **2** were tested against a panel of human cancer cell lines, namely, liver cancer cell line HepG2, colorectal adenocarcinoma cell line HT-29, malignant melanoma cell line A-375, colon cancer cell line HCT-116, lung carcinoma cell line A-549, and breast cancer line MDA-MB-231, as well as the noncancerous keratinocyte line HaCaT. Neither compound demonstrated cytotoxicity in the tested cancer cell lines. Both **1** and **2** were tested against a wide variety of Gram-positive and Gram-negative bacterial and fungal pathogens. They showed no inhibitory activity at the standard concentration of 100 μg mL^{-1} except a moderate activity against the plant pathogenic bacterium *Xanthomonas campestris* with IC_{50} values of 48 and 34 μM, respectively.

CONCLUSIONS

In this study, we have explored a cycad coralloid root symbiotic cyanobacterium for its novel secondary metabolites. This resulted in isolation and structure elucidation of the new lipoglycopeptides **1** and **2** and their aglycone **3**. We proposed that the *dsm* BGC is involved in the biosynthesis of these compounds. Desmamides feature an unprecedented type of fatty acyl moiety among lipopeptides, which is derived from a hexanoic acid starter unit. While the enzyme functions predicted to be encoded in the *dsm* BGC are congruent with the formation of **3** and, therefore, the aglycones of **1** and **2**, it was not possible to rationalize the glycosylating enzyme(s) through bioinformatics predictions. The desmamides expand the diversity of natural lipoglycopeptides, a small group of natural products with remarkable antibacterial and antifungal properties. We explored the biological activity of the desmamides and found that these were inactive toward several different human cancer cell lines. However, compound **2** showed antibiotic activity toward the black rot disease-causing plant pathogen *Xanthomonas campestris*. Lipopeptides and lipoglycopeptides often have important antibacterial activities.[17,44] Given their abundance in *D. muscorum* LEGE 12446, high concentrations of desmamides are likely to occur in a natural setting and could potentially be related to a defensive ecological role in its host plant. This will necessarily involve studying the potential production of **1**−**3** inside the coralloid roots. For example, two *Nostoc* sp. coralloid root endosymbionts, isolated from *Macrozamia* spp. cycads, were found to produce the toxin nodularin *in planta*.[45] Overall, the discovery of the desmamides and of the *dsm* BGC sets the foundation for exploring the role of these very abundant (1.6% d.w.) metabolites, in particular in the context of cycad coralloid root symbiosis. Despite all the recent progress in understanding the secondary metabolism of the facultative endosymbiont *Nostoc punctiforme* PCC 73102,[46] these systems are still poorly understood in terms of chemical ecology.[47]

EXPERIMENTAL SECTION

General Experimental Procedures. Optical rotations were measured using a JASCO P-2000 polarimeter with SpectraManager 2.14.02 software. Infrared spectra were collected on a Nicolet iS5 FTIR spectrometer (ThermoScientific) with OMNIC 9.8.372 software. The UV spectra were acquired on a UV-1600PC spectrometer (VWR) controlled by MWAVE 1.0.20 software. 1D and 2D NMR data were obtained in the Materials Center of the University of Porto (CEMUP) on a Bruker Avance III, 400 MHz, controlled by TopSpin 3.2. Compounds were analyzed in deuterated DMSO (DMSO-d_6, Sigma). Chemical shifts (^{1}H and ^{13}C) are expressed in δ (ppm), referenced to the residual nondeuterated solvent used (^{1}H, 2.500 ppm; ^{13}C, 39.52 ppm). NMR data were analyzed in MNova 12.0.4. LC-HRESIMS and LC-HRESIMS/MS analyses were performed on an UltiMate 3000 UHPLC (Thermo Fisher Scientific) system composed of an LPG-3400SD pump, WPS-3000SL autosampler, and VWD-3100 UV/vis detector coupled to a Q Exactive Focus Hybrid Quadrupole-Orbitrap mass spectrometer controlled by Q Exactive Focus Tune 2.9 and Xcalibur 4.1 (Thermo Fisher Scientific). For LC-HRESIMS data, full scan mode was used with the capillary voltage set to −3.8 kV, capillary temperature to 300 °C, and sheath gas flow rate to 35 units. HPLC separations were performed with a JASCO PU-4180 HPLC pump and an MD-4010 photodiode array detector, and separations were monitored at 254 nm wavelength. All solvents used were ACS grade, except for HPLC solvents (HPLC gradient grade) and LC-MS solvents (MS-grade). Stable-isotope-labeled fatty acids (d_{11}-hexanoic, d_{15}-octanoic, d_{19}-decanoic, and d_{23}-dodecanoic) were obtained from CDN Isotopes Inc.; amino acids were purchased from Fluorochem (D-allo-Thr; L-allo-Thr; D-Ser; L-Ser; L-Val; D-Val; L-Pro; D-Pro; D-Tyr; L-Tyr; D-Leu; L-Leu; D-Thr; L-Glu; D-Glu) and Glenthan Life Sciences (L-Thr). Monosaccharide standards were acquired from Sigma-Aldrich (D-xylose; L-arabinose), Alfa Aesar (D-ribose; D-arabinose), and Acros Organics (L-ribose). The reagent PMP was obtained from Alfa Aesar, and Nα-(2,4-dinitro-5-fluorophenyl)-L-alaninamide (Marfey's reagent) was purchased from Sigma-Aldrich.

https://doi.org/10.1021/acs.jnatprod.2c00162
J. Nat. Prod. 2022, 85, 1704−1714

Cyanobacterial Strain Cultivation. The cyanobacterial strain *Desmonostoc muscorum* LEGE 12446, kindly provided by LEGEcc,[26] was cultured in Z8 media, at 25 °C, with constant aeration, under a 14 h/10 h light (10−30 μmol photons s^{-1} m^{-2})/dark cycle. Large-scale culturing of this strain was carried out in 80 L low-density polyethylene sleeves for a total of 160 L, and cells were harvested during late exponential/early stationary phase (1.5−2 months of growth) through centrifugation (7178*g*), immediately frozen, and freeze-dried until further usage.

Molecular Networking Analysis. The cyanobacterial strain *D. muscorum* LEGE 12446 was analyzed using GNPS molecular networking analysis.[27] Briefly, 4 L of culture was harvested at the exponential phase of growth, frozen, and freeze-dried. An extraction of the dry cell material using a mixture of CH_2Cl_2/MeOH (2:1, v/v) was performed at room temperature, and the resulting extract was fractionated in a Strata SI-1 silica cartridge (5 g, 55 μm, 70A, Phenomenex) using a gradient of increasing polarity from *n*-hexane (*n*-hex) to EtOAc to MeOH, to yield three fractions (A−C). For LC-HRESIMS analysis, fractions were prepared at 1.0 mg mL^{-1} in LC-MS grade MeOH and filtered through a 0.2 μm syringe regenerated cellulose filter, and 5 μL was injected in an ACE Ultracore 2.5 SuperC18 column (75 × 2.1 mm). Samples were eluted at 0.35 mL min^{-1} over a linear gradient from 99.5% solution A (95% H_2O, 5% MeOH, 0.1% v/v HCOOH) and 0.5% solution B (95% isopropanol, 5% MeOH, 0.1% v/v HCOOH) to reach 10% solution B over 0.5 min, followed by an increase to 60% solution B in 8 min and then to 90% in 1 min; these conditions were kept for 6 min before returning to the initial conditions. The column oven was set to 40 °C, and UV monitoring was carried out at 254.0 nm. The capillary voltage of the heated electrospray ionization (HESI) was set to 3.8 kV and its temperature to 300 °C. The sheath gas and auxiliary gas flow rate were 35 and 10 (arbitrary units as provided by the software settings). Full MS scans were acquired at a resolution of 70 000 fwhm (range of 150−2000 *m*/*z*), and data-dependent MS/MS (ddMS^2, Discovery mode) at a resolution of 17,500 fwhm (isolation window used was 3.0 amu, and normalized collision energy was 35). For the molecular network analysis, the protocol available in GNPS documentation was followed and the resulting network file was visualized using Cytoscape v3.8.0.

Extraction and Isolation of 1−3. Freeze-dried biomass from large-scale culturing (70.3 g, d.w.) was extracted by repeated percolation using a mixture of CH_2Cl_2/MeOH (2:1, v/v) at room temperature and at 40 °C. A total extract mass of 14.7 g was obtained. Further fractionation using VLC was performed, using silica gel 60 (0.015−0.040 mm, Merck). The extract was dry loaded onto the column using 15 g of silica. A mixture of 1:1 (v/v) EtOAc/*n*-hex was used to start the separation, and a stepwise gradient to 100% EtOAc and then to 100% MeOH was used, yielding 13 fractions. Fractions containing the mass features of interest (eluting with 2:3 (v/v) to 3:7 (v/v) EtOAc/MeOH) were further fractionated using flash chromatography (silica gel 60, 0.040−0.063 mm, Merck), with a stepwise gradient from 1:1 (v/v) EtOAc/MeOH to 100% MeOH, yielding seven fractions. The mass features of interest were present in fractions 2−4, which were pooled and further separated by reversed-phase solid phase extraction (SPE) in a Strata C18-E cartridge (50g, 55 μm, 70A, Phenomenex) using a stepwise gradient from 5% MeOH(aq) (solution A) to 95% isopropyl alcohol (IPA) with 5% MeOH (solution B), yielding a total of 11 fractions. The first fraction (A, 565 mg), eluting with 5% MeOH(aq), was selected for reversed-phase semipreparative HPLC separation using a C18 column (100 Å, 250 × 10 mm, 5 μm, ACE). A gradient elution program was employed, starting with 35% MeCN(aq), increasing to 60% MeCN(aq) over 20 min, and then to 100% MeCN in 5 min, before returning to the initial conditions. Fraction A2 (33.5 mg, t_R 8−9 min) was collected and subjected to an additional purification step in the same system but with a gradient starting at 35% MeCN(aq) and increasing to 46% MeCN(aq) in 15 min and then to 100% MeCN in 5 min before returning to the initial conditions. This purified fraction A2 corresponded to spectroscopically pure desmamide A (compound **1**, t_R = 10.0 min, 26.3 mg). HPLC fraction A5 (5.8 mg, t_R = 11−13 min) corresponded to partially purified desmamide C and was further separated by semipreparative reversed-phase HPLC with an Aeris Peptide XB-C18 column (100 Å, 250 × 10 mm, 5 μm, Phenomenex). A gradient from 35% MeCN(aq) to 45% MeCN(aq) in 22 min was applied to yield spectroscopically pure desmamide C (**3**, t_R = 15.5 min, 4.0 mg). Desmamide B (**2**) was purified from SPE fraction E (977 mg), eluting with a 3:2 (v/v) mixture of solution A (5% MeOH(aq)) and solution B (IPA with 5% MeOH), following semipreparative HPLC using an Aeris Peptide XB-C18 column (100 Å, 250 × 10 mm, 5 μm, Phenomenex). The separation was carried out with isocratic 35% MeCN(aq) for 16 min and then a linear gradient to 50% MeCN(aq) in 3 min, before returning to the initial conditions. Only 205 mg of sample (fraction E) was processed. Fraction E6 corresponded to spectroscopically pure desmamide B (**2**, t_R = 18.0 min, 20.4 mg).

Desmamide A (1). Amorphous white powder; $[\alpha]_D^{23}$ +41 (*c* 0.01, MeOH); UV (MeOH) λ_{max} (log ε) 219 (3.2), 272 (2.9), 279 (2.8); IR ν_{max} 3271, 2955, 2930, 2930, 2871, 2351, 2318, 1739, 1733, 1667, 1661, 1652, 1645, 1635, 1574, 1557, 1549, 1539, 1532, 1512, 1455, 1418 cm^{-1}; ^1H and ^{13}C NMR spectroscopic data (DMSO-d_6), Table 1; HRESIMS *m*/*z* 1388.7577 $[M + H]^+$ (calcd for $C_{66}H_{106}N_{11}O_{21}$, 1388.7559); HRESIMS/MS (Figure S13).

Desmamide B (2). Amorphous white powder; $[\alpha]_D^{23}$ +37 (*c* 0.01, MeOH); UV (MeOH) λ_{max} (log ε) 222 (3.2), 272 (2.9), 279 (2.8); IR ν_{max} 3271, 2954, 2929, 2870, 2351, 2328, 1738, 1733, 1667, 1660, 1651, 1645, 1634, 1574, 1557, 1548, 1539, 1532, 1512, 1463, 1418 cm^{-1}; ^1H and ^{13}C NMR spectroscopic data (DMSO-d_6), Table S3; HRESIMS *m*/*z* 1430.7666 $[M + H]^+$ (calcd for $C_{68}H_{108}N_{11}O_{22}$, 1430.7665); HRESIMS/MS (Figure S27).

Desmamide C (3). Amorphous white powder; $[\alpha]_D^{23}$ +10 (*c* 0.01, MeOH); UV (MeOH) λ_{max} (log ε) 231 (3.2), 278 (3.1); IR ν_{max} 3271, 2956, 2929, 2871, 2351, 1660, 1651, 1539, 1516, 1447 cm^{-1}; ^1H and ^{13}C NMR spectroscopic data (DMSO-d_6), Table S4, Figures S21, S22; HRESIMS *m*/*z* 1256.7149 $[M + H]^+$ (calcd for $C_{61}H_{98}N_{11}O_{17}$, 1256.7142); HRESIMS/MS (Figure S28).

HRESIMS/MS Analysis. HRESIMS/MS analysis of pure **1**−**3** was performed by direct injection of each compound (1.0 mg mL^{-1}, flow 0.005 mL min^{-1}) into the spectrometer, with a 35 000 fwhm resolution, using an isolation window of 1 *m*/*z*, loop count of 3, AGC target of 5 × 10^4, and a collision energy of 60 (arbitrary units).

Quantification of Desmamides in *D. muscorum* LEGE 12446. To quantify the production of desmamides in the cyanobacterial *D. muscorum* LEGE 12446, a calibration curve for each compound was obtained from LC-HRESIMS analysis. Briefly, desmamide A−C standards were prepared at 0.5, 0.1, 0.05, 0.01, 0.005, and 0.001 mg mL^{-1}. Five microliters (5 μL) of each standard solution was injected in an LC-HRESIMS system fitted with an ACE Ultracore 2.5 SuperC18 column (75 × 2.1 mm) following the same chromatographic and spectrometric conditions described in the molecular networking analysis method. The area under the curve from the extracted ion chromatograms (EIC) for each compound was plotted (0.1 to 0.001 mg mL^{-1}), and a linear regression was fitted. This was then used to extrapolate the concentration of each compound in the initial extract used for isolation and in the biomass from which it was obtained (Table S2, Figure S3).

Chiral-Phase HPLC. For the acid hydrolysis of **1**, 1.5 mg of compound was placed into 1.0 mL of 6 N HCl for 24 h at 110 °C under continuous stirring. After the reaction, HCl was removed under a N_2 stream. Amino acids standards (proline, valine, leucine, tyrosine), L- and D- isomers, were prepared at 0.5 mg mL^{-1} with MS-grade H_2O. The hydrolysate of **1** was prepared at 1.0 mg mL^{-1} with MS-grade H_2O. A volume of 10 μL of each sample was injected onto the HPLC system and separated on a Chirex 3126 (D)-penicillamine column (50 × 4.6 mm, Phenomenex), using a 1 mM $CuSO_4/H_2O$ solution as mobile phase, at a 1.0 mL min^{-1} flow rate. To confirm the absolute configurations of the amino acids, co-injection of the hydrolysate with both versions of each amino acid standard (15 μL + 5 μL, respectively) was performed. Retention times (t_R, min) for standards: L-Pro 4.7, D-Pro 9.7, L-Val 6.4, D-Val 11.1, L-

https://doi.org/10.1021/acs.jnatprod.2c00162
J. Nat. Prod. 2022, 85, 1704−1714

Leu 21.3, D-Leu 34.5, L-Tyr 24.0, and D-Tyr 43.8. Retention times (t_R, min) for hydrolysate: L-Pro 4.4, L-Val 5.9, D-Leu 32.5, and D-Tyr 42.3.

Marfey's Derivatization Analysis. The Marfey's derivatization method was used to assign the configuration of Ser, Gln, Thr, and *allo*-Thr residues. L- and D- Isomer standards of each amino acid were prepared at 50 mM in 50 μL of LC-MS-grade H_2O. For the Gln residue, standards where prepared using L-Glu and D-Glu. A Marfey's reagent (1-fluoro-2,4-dinitrophenyl-5-L-alanine amide) solution was prepared at a 1% (w/v) concentration in 100 μL of acetone. For hydrolysate (0.6 mg, obtained as for the chiral-phase HPLC analysis) derivatization, 100 μL of 1 M $NaHCO_3$ and 100 μL of the Marfey's reagent acetone solution were added to a glass vial, which was placed on an oil bath at 40 °C for 1 h with a magnetic stirrer. The reaction was quenched with 100 μL of 1 M HCl, diluted with 200 μL of MeCN (LC-MS grade), and filtered (0.2 μm). The same protocol was applied to the amino acid standards: to 50 μL of each standard were added 20 μL of 1 M $NaHCO_3$ and 100 μL of the Marfey's reagent solution. The reaction (40 °C, 1 h) was quenched with 20 μL of 1 M HCl and diluted with 810 μL of MeCN. After derivatization all samples were analyzed by LC-HRESIMS, using an ACE UltraCore 2.5 SuperC18 column (75 × 2.1 mm, Avantor). Eluents were solutions A (95% H_2O, 5% MeOH, 0.1% v/v HCOOH) and B (95% IPA, 5% MeOH, 0.1% v/v HCOOH). The separation was carried out as follows: 100% A for 1 min, then a linear gradient for 7 min to 60% B, and then a steeper gradient to 100% B in 1 min, and held at 100% B for 2 min before returning to the initial conditions. The injection volume was 10 μL. Retention times (t_R, min) for standards: L-Ser 7.29, D-Ser 7.35, L-Leu 12.04, D-Leu 13.61, L-Thr 10.29, D-Thr 16.84, L-*allo*-Thr 10.50, D-allo-Thr 12.87, L-Glu 5.13, and D-Glu 5.47. Retention times (t_R, min) for hydrolysate: L-Ser 7.29, D-Leu 13.62, L-Thr 10.23, and D-Glu 5.54.

Incubation Experiments with Perdeuterated Fatty Acids. To study the putative incorporation of a fatty acid unit in desmamide A, supplementation of *Desmonostoc muscorum* LEGE 12446 with a series of deuterium-labeled fatty acids—d_{11}-hexanoic acid (d_{11}-C6), d_{15}-octanoic acid (d_{15}-C8), d_{19}-decanoic acid (d_{19}-C10), and d_{23}-dodecanoic acid (d_{23}-C12)—was carried out. Stock solutions of the labeled fatty acids were prepared in DMSO (500 mM). Small-scale cultures (25 mL) growing in Z8 medium were supplemented with pulse additions (three times, two-day interval) of 8.33 μL of deuterated fatty acid stock solution, to a final concentration of 0.5 mM. A control experiment with nondeuterated hexanoic acid (C6) was performed. Experiments were carried out in duplicate. Cultures were placed in the same growth conditions described above with shaking in an orbital shaker at 200 rpm. After 7 days, cells were harvested by centrifugation, and the pellet was rinsed with ddH2O and extracted with 15 mL of a mixture of CH_2Cl_2/MeOH (2:1, v/v) in an orbital shaker for 30 min. The extracts were then filtered, dried under vacuum, and resuspended in MeOH for LC-HRESIMS analysis (2 mg mL^{-1}). Samples were separated on an ACE UltraCore SuperC18 (2.5 μm, 95 Å, 75 × 2.1 mm) column. Elution was performed with a 0.4 mL min^{-1} flow using mixtures of eluents A (H_2O/MeOH, 1:1, 0.1% v/v HCOOH) and B (IPA, 0.1% v/v HCOOH). The following program was applied: isocratic 10% B for 1 min, then a linear gradient to 65% B over 5 min, holding at 65% B for 12 min before increasing to 85% B over 2 min, and holding again for 9 min at 85% B before returning to the initial conditions. The column oven was set to 40 °C, and data were obtained in full scan (switching mode), with a capillary voltage of HESI +3.5 kV/−3.8 kV and a capillary temperature of 300 °C.

Monosaccharide Derivatization Analysis with PMP. To determine the identity of the sugar residue in **1**, we used a sugar derivatization method using PMP to allow for LC-MS-based determination of monosaccharides.[48] Some adaptations to the published method were made. Briefly, monosaccharide standards (D-arabinose, D-xylose, and D-ribose) were prepared at 0.5 mg mL^{-1} with LC-MS-grade H_2O. To 100 μL of each sugar solution were added 100 μL of 0.3 M NaOH and 100 μL of PMP reagent (0.5 M in MeOH). Reaction mixtures were placed in an oil bath at 70 °C for 30 min. The mixtures were then quenched with 100 μL of 0.3 M HCl and dried in a rotatory evaporator. Equal volumes of H_2O and $CHCl_3$ (1 mL) were added to extract the PMP residues. The organic layer was discarded, and this process was repeated twice by adding $CHCl_3$ to the aqueous layer. Finally, the aqueous layer was dried and dissolved using 1 mL of LC-MS-grade H_2O. The same protocol was applied to 0.5 mg of the hydrolysate of **1**, which was dissolved in 0.5 mL of LC-MS-grade H_2O. For monosaccharide derivative analysis, an LC-HRESIMS run was performed, using an ACE UltraCore SuperC18 (2.5 μm, 95 Å, 75 × 2.1 mm) column, and the elution was carried out isocratically with a 83:17 v/v mixture of H_2O with 0.1% v/v HCOOH and MeCN with 0.1% v/v HCOOH, respectively. The flow rate used was 0.4 mL min^{-1}, 5 μL of each derivative monosaccharide and hydrolysate solution were injected for analysis, and the separation was monitored using a wavelength of 245 nm. The column oven was set to 30 °C. Retention times (t_R, min) for standards: ribose 5.1, arabinose 10.7, xylose 11.5. Retention times (t_R, min) for hydrolysate: arabinose 10.7 (minor) and xylose 11.4 (major).

Genome Sequencing and Bioinformatics Analysis. The cyanobacterium *D. muscorum* LEGE 12446 was sequenced through a specialized sequencing service (enhanced genome service) provided by the company MicrobesNG, using a combination of short-read Illumina and long-read nanopore sequencing technologies. Fresh biomass, harvested after 15 days' cultivation period, was sent to the service provider. Following gDNA extraction and sequencing, raw data were submitted to a bioinformatics pipeline. Briefly, identification of the closest reference genomes for reading mapping was done using Kraken 2,[49] BWA-MEM was used to check the quality of the reads, and *de novo* assembly was performed using SPAdes.[50] Because the culture was not axenic, the genomic data were treated as a metagenome: the retrieved contigs were analyzed using the binning tool MaxBin 2.0.[51] This procedure yielded a nearly complete genome (GenBank: JADEXS020000000) with an estimated size of 9.64 Mb, distributed among 12 contigs. AntiSMASH v6.0[37] was used to annotate BGCs in the genome data using relaxed detection settings and all extra features selected. Manual annotation and searches for enzyme homologues in the genome of *D. muscorum* LEGE 12446 were performed using BlastP or tBlastn.

Cell Viability Assay. The sensitivity of malignant melanoma cell line A-375 (CLS), colon cancer cell line HCT-116 (DSMZ), lung carcinoma cell line A-549 (CLS), human breast cancer line MDA-MB-231 (CLS), and the noncancerous human keratinocyte line HaCaT (CLS) to the samples was evaluated by monitoring the metabolic activity using the CellTiterBlue cell viability assay (Promega). HaCaT cells were cultivated in RPMI medium, A549 and MDA-MB-231 cells in DMEM:Ham's F12 medium (1:1) supplemented with 15 mM HEPES, and A-375 and HCT-116 cells in DMEM medium supplemented with 4.5 g L^{-1} D-glucose and 110 mg L^{-1} sodium pyruvate. All media were supplemented with L-glutamine, 10% fetal bovine serum, 100 U mL^{-1} penicillin, and 100 mg mL^{-1} streptomycin. The cultures were maintained at 37 °C under a humidified atmosphere and 5% CO_2. The cell lines were transferred every 3 or 4 days. For experimental procedures, cells were seeded in 96-well plates at a concentration of 10 00 cells per well in RPMI. After 24 h of incubation, the medium was removed, and 100 μL of fresh medium including the test sample was added to the cells. A 100 μg mL^{-1} concentration of doxorubicin, as a standard therapeutic drug, was used as a positive control. Following compound addition, plates were cultured for 24 h at 37 °C. Afterward, the assay was performed according to the manufacturer's instructions of the CellTiterBlue viability assay and measured using a Tecan Infinite M200 microplate reader at an excitation of 560 nm and emission of 590 nm. The IC_{50} value was calculated as the concentration that shows 50% inhibition of the viability.

Antibacterial Assay. The antimicrobial assay was performed using *Xanthomonas campestris* DSM 2405. The cultivation took place in TSB medium (1.2% tryptic soy broth; 0.5% NaCl). An overnight culture of the test organism was prepared and diluted to an optical density (600 nm) of 0.03. To prepare the assay, the samples (20 mg mL^{-1} stock solution) were dissolved in medium and transferred into a 96-well microtiter plate, and 200 μL of the diluted culture was added

https://doi.org/10.1021/acs.jnatprod.2c00162
J. Nat. Prod. 2022, 85, 1704−1714

to each well. The inoculated microplate was incubated for 7 h at 28 °C and 200 rpm. To detect the inhibitory effect of the substances, 10 μL of a resazurin solution (0.3 mg mL^{-1} phosphate-buffered saline) was added to the microplate and incubated again for 1 h, and the fluorescence signal (560 nm/590 nm) was measured using the Tecan Infinite M200 microplate reader. Chloramphenicol was used as the positive control. The IC_{50} value was calculated as the concentration that shows 50% inhibition of the viability.

■ ASSOCIATED CONTENT

Supporting Information

The Supporting Information is available free of charge at https://pubs.acs.org/doi/10.1021/acs.jnatprod.2c00162.

GNPS molecular networking of *Desmonostoc muscorum* LEGE 12446; fractionation scheme and quantification of desmamides production in the cyanobacterium; ^{1}H, ^{13}C, COSY, HSQC, HMBC, NOESY, HRESIMS, HRESIMS/MS, and FT-IR spectra of **1**; PMP sugar and Marfey's derivatization of **1**; chiral-phase analysis of **1**; NMR table, ^{1}H, ^{13}C, COSY, HSQC, HMBC, HRESIMS/MS, and FT-IR spectra of **2**; NMR table, ^{1}H, ^{13}C, HRESIMS/MS, and FT-IR spectra of **3**; HRESIMS/MS spectra comparison between desmamide aglycones (**1** and **2**) with **3**; annotation of the *dsm* BGC and tBlastn search of glycosyltransferases; lipoglycopeptide structural diversity; biological activities of **1** and **2** (PDF)

■ AUTHOR INFORMATION

Corresponding Author

Pedro N. Leão − *Interdisciplinary Centre of Marine and Environmental Research (CIIMAR/CIMAR), University of Porto, 4450-208 Matosinhos, Portugal;* orcid.org/0000-0001-5064-9164; Email: pleao@ciimar.up.pt

Authors

Sara Freitas − *Interdisciplinary Centre of Marine and Environmental Research (CIIMAR/CIMAR), University of Porto, 4450-208 Matosinhos, Portugal; Department of Biology, Faculty of Sciences, University of Porto Rua do Campo Alegre, 4169-007 Porto, Portugal*

Raquel Castelo-Branco − *Interdisciplinary Centre of Marine and Environmental Research (CIIMAR/CIMAR), University of Porto, 4450-208 Matosinhos, Portugal*

Arlette Wenzel-Storjohann − *GEOMAR Centre for Marine Biotechnology (GEOMAR-Biotech), Research Unit Marine Natural Product Chemistry, GEOMAR Helmholtz Centre for Ocean Research Kiel, 24106 Kiel, Germany*

Vitor M. Vasconcelos − *Interdisciplinary Centre of Marine and Environmental Research (CIIMAR/CIMAR), University of Porto, 4450-208 Matosinhos, Portugal; Department of Biology, Faculty of Sciences, University of Porto Rua do Campo Alegre, 4169-007 Porto, Portugal*

Deniz Tasdemir − *GEOMAR Centre for Marine Biotechnology (GEOMAR-Biotech), Research Unit Marine Natural Product Chemistry, GEOMAR Helmholtz Centre for Ocean Research Kiel, 24106 Kiel, Germany; Kiel University, 24118 Kiel, Germany;* orcid.org/0000-0002-7841-6271

Complete contact information is available at: https://pubs.acs.org/10.1021/acs.jnatprod.2c00162

Notes

The authors declare no competing financial interest.

The genome sequence of *D. muscorum* LEGE 12446 is available at GenBank (Accession: JADEXS020000000). The GNPS data set is available in MassIVE (MSV000088770). HRESIMS/MS spectra for **1**−**3** have been added to the GNPS Library under accessions CCMSLIB00009918389, CCMSLIB00009918390, and CCMSLIB00009918391, respectively. NMR data for **1**−**3** are available at DOI: 10.6084/m9.figshare.19119107.

■ ACKNOWLEDGMENTS

We thank the support of Fundação para a Ciência e a Tecnologia (FCT) through grants UIDB/04423/2020 and UIDP/04423/2020 and scholarships SFRH/BD/116009/2016 to S.F. and SFRH/BD/136367/2018 to R.C.B. This work has received funding from the European Union's Horizon 2020 research and innovation program under grant agreement No. 952374 and from grant ATLANTIDA (ref NORTE-01-0145-FEDER-000040), supported by NORTE2020 and European Regional Development Fund (ERDF).

■ REFERENCES

(1) Gaysina, L. A.; Saraf, A.; Singh, P.. In *Cyanobacteria*; Elsevier, 2019; pp 1−28.
(2) Haselkorn, R. *Annu. Rev. Plant Physiol.* **1978**, *29*, 319−344.
(3) Chang, A. C. G.; Chen, T.; Li, N.; Duan, J. *Front. Microbiol.* **2019**, *10*, 1888.
(4) Lindblad, P. In *Prokaryotic Symbionts in Plants*; Pawlowski, K., Ed.; Springer Berlin Heidelberg: Berlin, Heidelberg, 2008; Vol. *8*, pp 225−233.
(5) NCBI Genome (accessed 29 Jan 2022).
(6) Popin, R. V.; Alvarenga, D. O.; Castelo-Branco, R.; Fewer, D. P.; Sivonen, K. *Front. Microbiol.* **2021**, *12*, 684565.
(7) Shih, P. M.; Wu, D.; Latifi, A.; Axen, S. D.; Fewer, D. P.; Talla, E.; Calteau, A.; Cai, F.; Tandeau de Marsac, N.; Rippka, R.; Herdman, M.; Sivonen, K.; Coursin, T.; Laurent, T.; Goodwin, L.; Nolan, M.; Davenport, K. W.; Han, C. S.; Rubin, E. M.; Eisen, J. A.; Woyke, T.; Gugger, M.; Kerfeld, C. A. *Proc. Natl. Acad. Sci. U. S. A.* **2013**, *110*, 1053−1058.
(8) Moore, B. S.; Chen, J. L.; Patterson, G. M. L.; Moore, R. E.; Brinen, L. S.; Kato, Y.; Clardy, J. *J. Am. Chem. Soc.* **1990**, *112*, 4061−4063.
(9) Hohlman, R. M.; Sherman, D. H. *Nat. Prod. Rep.* **2021**, *38*, 1567−1588.
(10) Schwartz, R. E.; Hirsch, C. F.; Sesin, D. F.; Flor, J. E.; Chartrain, M.; Fromtling, R. E.; Harris, G. H.; Salvatore, M. J.; Liesch, J. M.; Yudin, K. *J. Ind. Microbiol.* **1990**, *5*, 113−123.
(11) Proteau, P. J.; Gerwick, W. H.; Garcia-Pichel, F.; Castenholz, R. *Experientia* **1993**, *49*, 825−829.
(12) Kaasalainen, U.; Fewer, D. P.; Jokela, J.; Wahlsten, M.; Sivonen, K.; Rikkinen, J. *Proc. Natl. Acad. Sci. U. S. A.* **2012**, *109*, 5886−5891.
(13) Liaimer, A.; Jensen, J. B.; Dittmann, E. *Front. Microbiol.*, DOI: 10.3389/fmicb.2016.01693.
(14) Liaimer, A.; Jenke-Kodama, H.; Ishida, K.; Hinrichs, K.; Stangeland, J.; Hertweck, C.; Dittmann, E. *Environ. Microbiol. Rep.* **2011**, *3*, 550−558.
(15) Liaimer, A.; Helfrich, E. J. N.; Hinrichs, K.; Guljamow, A.; Ishida, K.; Hertweck, C.; Dittmann, E. *Proc. Natl. Acad. Sci. U. S. A.* **2015**, *112*, 1862−1867.
(16) Fewer, D. P.; Jokela, J.; Heinilä, L.; Aesoy, R.; Sivonen, K.; Galica, T.; Hrouzek, P.; Herfindal, L. *Physiol. Plant.* **2021**, *173*, 639−650.
(17) Kahne, D.; Leimkuhler, C.; Lu, W.; Walsh, C. *Chem. Rev.* **2005**, *105*, 425−448.
(18) Tyurin, A. P.; Alferova, V. A.; Paramonov, A. S.; Shuvalov, M. V.; Kudryakova, G. K.; Rogozhin, E. A.; Zherebker, A. Y.; Brylev, V. A.; Chistov, A. A.; Baranova, A. A.; Biryukov, M. V.; Ivanov, I. A.; Prokhorenko, I. A.; Grammatikova, N. E.; Kravchenko, T. V.; Isakova,

E. B.; Mirchink, E. P.; Gladkikh, E. G.; Svirshchevskaya, E. V.; Mardanov, A. V.; Beletsky, A. V.; Kocharovskaya, M. V.; Kulyaeva, V. V.; Shashkov, A. S.; Tsvetkov, D. E.; Nifantiev, N. E.; Apt, A. S.; Majorov, K. B.; Efimova, S. S.; Ravin, N. V.; Nikolaev, E. N.; Ostroumova, O. S.; Katrukha, G. S.; Lapchinskaya, O. A.; Dontsova, O. A.; Terekhov, S. S.; Osterman, I. A.; Shenkarev, Z. O.; Korshun, V. A. *Angew. Chem., Int. Ed.* **2021**, *60*, 18694−18703.
(19) Bui, T.-H.; Wray, V.; Nimtz, M.; Fossen, T.; Preisitsch, M.; Schröder, G.; Wende, K.; Heiden, S. E.; Mundt, S. *J. Nat. Prod.* **2014**, *77*, 1287−1296.
(20) Vestola, J.; Shishido, T. K.; Jokela, J.; Fewer, D. P.; Aitio, O.; Permi, P.; Wahlsten, M.; Wang, H.; Rouhiainen, L.; Sivonen, K. *Proc. Natl. Acad. Sci. U. S. A.* **2014**, *111*, E1909−E1917.
(21) Somma, S.; Gastaldo, L.; Corti, A. *Antimicrob. Agents Chemother.* **1984**, *26*, 917−923.
(22) Singh, M. P.; Petersen, P. J.; Weiss, W. J.; Janso, J. E.; Luckman, S. W.; Lenoy, E. B.; Bradford, P. A.; Testa, R. T.; Greenstein, M. *Antimicrob. Agents Chemother.* **2003**, *47*, 62−69.
(23) Ciabatti, R.; Kettenring, J. K.; Winters, G.; Tuan, G.; Zerilli, L.; Cavalleri, B. *J. Antibiot. (Tokyo)* **1989**, *42*, 254−267.
(24) Lu, S.-E.; Novak, J.; Austin, F. W.; Gu, G.; Ellis, D.; Kirk, M.; Wilson-Stanford, S.; Tonelli, M.; Smith, L. *Biochemistry* **2009**, *48*, 8312−8321.
(25) Butler, M. S.; Hansford, K. A.; Blaskovich, M. A. T.; Halai, R.; Cooper, M. A. *J. Antibiot. (Tokyo)* **2014**, *67*, 631−644.
(26) Ramos, V.; Morais, J.; Castelo-Branco, R.; Pinheiro, Â.; Martins, J.; Regueiras, A.; Pereira, A. L.; Lopes, V. R.; Frazão, B.; Gomes, D.; Moreira, C.; Costa, M. S.; Brûle, S.; Faustino, S.; Martins, R.; Saker, M.; Osswald, J.; Leão, P. N.; Vasconcelos, V. M. *J. Appl. Phycol.* **2018**, *30*, 1437−1451.
(27) Wang, M.; Carver, J. J.; Phelan, V. V.; Sanchez, L. M.; Garg, N.; Peng, Y.; Nguyen, D. D.; Watrous, J.; Kapono, C. A.; Luzzatto-Knaan, T.; Porto, C.; Bouslimani, A.; Melnik, A. V.; Meehan, M. J.; Liu, W.-T.; Crüsemann, M.; Boudreau, P. D.; Esquenazi, E.; Sandoval-Calderón, M.; Kersten, R. D.; Pace, L. A.; Quinn, R. A.; Duncan, K. R.; Hsu, C.-C.; Floros, D. J.; Gavilan, R. G.; Kleigrewe, K.; Northen, T.; Dutton, R. J.; Parrot, D.; Carlson, E. E.; Aigle, B.; Michelsen, C. F.; Jelsbak, L.; Sohlenkamp, C.; Pevzner, P.; Edlund, A.; McLean, J.; Piel, J.; Murphy, B. T.; Gerwick, L.; Liaw, C.-C.; Yang, Y.-L.; Humpf, H.-U.; Maansson, M.; Keyzers, R. A.; Sims, A. C.; Johnson, A. R.; Sidebottom, A. M.; Sedio, B. E.; Klitgaard, A.; Larson, C. B.; Boya, C. A.; Torres-Mendoza, P. D.; Gonzalez, D. J.; Silva, D. B.; Marques, L. M.; Demarque, D. P.; Pociute, E.; O'Neill, E. C.; Briand, E.; Helfrich, E. J. N.; Granatosky, E. A.; Glukhov, E.; Ryffel, F.; Houson, H.; Mohimani, H.; Kharbush, J. J.; Zeng, Y.; Vorholt, J. A.; Kurita, K. L.; Charusanti, P.; McPhail, K. L.; Nielsen, K. F.; Vuong, L.; Elfeki, M.; Traxler, M. F.; Engene, N.; Koyama, N.; Vining, O. B.; Baric, R.; Silva, R. R.; Mascuch, S. J.; Tomasi, S.; Jenkins, S.; Macherla, V.; Hoffman, T.; Agarwal, V.; Williams, P. G.; Dai, J.; Neupane, R.; Gurr, J.; Rodríguez, A. M. C.; Lamsa, A.; Zhang, C.; Dorrestein, K.; Duggan, B. M.; Almaliti, J.; Allard, P.-M.; Phapale, P.; Nothias, L.-F.; Alexandrov, T.; Litaudon, M.; Wolfender, J.-L.; Kyle, J. E.; Metz, T. O.; Peryea, T.; Nguyen, D.-T.; VanLeer, D.; Shinn, P.; Jadhav, A.; Müller, R.; Waters, K. M.; Shi, W.; Liu, X.; Zhang, L.; Knight, R.; Jensen, P. R.; Palsson, B. Ø.; Pogliano, K.; Linington, R. G.; Gutiérrez, M.; Lopes, N. P.; Gerwick, W. H.; Moore, B. S.; Dorrestein, P. C.; Bandeira, N. *Nat. Biotechnol.* **2016**, *34*, 828−837.
(28) Mohimani, H.; Gurevich, A.; Mikheenko, A.; Garg, N.; Nothias, L.-F.; Ninomiya, A.; Takada, K.; Dorrestein, P. C.; Pevzner, P. A. *Nat. Chem. Biol.* **2017**, *13*, 30−37.
(29) Gurevich, A.; Mikheenko, A.; Shlemov, A.; Korobeynikov, A.; Mohimani, H.; Pevzner, P. A. *Nat. Microbiol.* **2018**, *3*, 319−327.
(30) Mohimani, H.; Gurevich, A.; Shlemov, A.; Mikheenko, A.; Korobeynikov, A.; Cao, L.; Shcherbin, E.; Nothias, L.-F.; Dorrestein, P. C.; Pevzner, P. A. *Nat. Commun.* **2018**, *9*, 4035.
(31) Dictionary of Natural Products 32.0, https://dnp.chemnetbase.com, (accessed 20 Dec 2021).
(32) van Santen, J. A.; Jacob, G.; Singh, A. L.; Aniebok, V.; Balunas, M. J.; Bunsko, D.; Neto, F. C.; Castaño-Espriu, L.; Chang, C.; Clark, T. N.; Cleary Little, J. L.; Delgadillo, D. A.; Dorrestein, P. C.; Duncan, K. R.; Egan, J. M.; Galey, M. M.; Haeckl, F. P. J.; Hua, A.; Hughes, A. H.; Iskakova, D.; Khadilkar, A.; Lee, J.-H.; Lee, S.; LeGrow, N.; Liu, D. Y.; Macho, J. M.; McCaughey, C. S.; Medema, M. H.; Neupane, R. P.; O'Donnell, T. J.; Paula, J. S.; Sanchez, L. M.; Shaikh, A. F.; Soldatou, S.; Terlouw, B. R.; Tran, T. A.; Valentine, M.; van der Hooft, J. J. J.; Vo, D. A.; Wang, M.; Wilson, D.; Zink, K. E.; Linington, R. G. *ACS Cent. Sci.* **2019**, *5*, 1824−1833.
(33) Claridge, T. D. W.; Pérez-Victoria, I. *Org. Biomol Chem.* **2003**, *1*, 3632−3634.
(34) Usvalampi, A. Doctoral thesis, School of Chemical Technology, 2013.
(35) Zhang, Y.; Liu, S.; Liu, H.; Liu, X.; Che, Y. *J. Nat. Prod.* **2009**, *72*, 1364−1367.
(36) Ortiz-López, F. J.; Carretero-Molina, D.; Sánchez-Hidalgo, M.; Martín, J.; González, I.; Román-Hurtado, F.; Cruz, M.; García-Fernández, S.; Reyes, F.; Deisinger, J. P.; Müller, A.; Schneider, T.; Genilloud, O. *Angew. Chem., Int. Ed.* **2020**, *59*, 12654−12658.
(37) Blin, K.; Shaw, S.; Kloosterman, A. M.; Charlop-Powers, Z.; van Wezel, G. P.; Medema, M. H.; Weber, T. *Nucleic Acids Res.* **2021**, *49*, W29−W35.
(38) Keatinge-Clay, A. T. *Chem. Biol.* **2007**, *14*, 898−908.
(39) Fischbach, M. A.; Walsh, C. T. *Chem. Rev.* **2006**, *106*, 3468−3496.
(40) Magarvey, N. A.; Haltli, B.; He, M.; Greenstein, M.; Hucul, J. A. *Antimicrob. Agents Chemother.* **2006**, *50*, 2167−2177.
(41) Favrot, L.; Blanchard, J. S.; Vergnolle, O. *Biochemistry* **2016**, *55*, 989−1002.
(42) Daigle, D. M.; Hughes, D. W.; Wright, G. D. *Chem. Biol.* **1999**, *6*, 99−110.
(43) Hegde, S. S.; Javid-Majd, F.; Blanchard, J. S. *J. Biol. Chem.* **2001**, *276*, 45876−45881.
(44) Hamley, I. W. *Chem. Commun.* **2015**, *51*, 8574−8583.
(45) Gehringer, M. M.; Adler, L.; Roberts, A. A.; Moffitt, M. C.; Mihali, T. K.; Mills, T. J. T.; Fieker, C.; Neilan, B. A. *ISME J.* **2012**, *6*, 1834−1847.
(46) Dehm, D.; Krumbholz, J.; Baunach, M.; Wiebach, V.; Hinrichs, K.; Guljamow, A.; Tabuchi, T.; Jenke-Kodama, R. D.; Süssmuth; Dittmann, E. *ACS Chem. Biol.*, DOI: 10.1021/acschembio.9b00240.
(47) Gutiérrez-García, K.; Bustos-Díaz, E. D.; Corona-Gómez, J. A.; Ramos-Aboites, H. E.; Sélem-Mojica, N.; Cruz-Morales, P.; Pérez-Farrera, M. A.; Barona-Gómez, F.; Cibrián-Jaramillo, A. *Genome Biol. Evol.* **2019**, *11*, 319−334.
(48) Honda, S.; Akao, E.; Suzuki, S.; Okuda, M.; Kakehi, K.; Nakamura, J. *Anal. Biochem.* **1989**, *180*, 351−357.
(49) Wood, D. E.; Salzberg, S. L. *Genome Biol.* **2014**, *15*, R46.
(50) Bankevich, A.; Nurk, S.; Antipov, D.; Gurevich, A. A.; Dvorkin, M.; Kulikov, A. S.; Lesin, V. M.; Nikolenko, S. I.; Pham, S.; Prjibelski, A. D.; Pyshkin, A. V.; Sirotkin, A. V.; Vyahhi, N.; Tesler, G.; Alekseyev, M. A.; Pevzner, P. A. *J. Comput. Biol.* **2012**, *19*, 455−477.
(51) Wu, Y.-W.; Simmons, B. A.; Singer, S. W. *Bioinformatics* **2016**, *32*, 605−607.

https://doi.org/10.1021/acs.jnatprod.2c00162
J. Nat. Prod. 2022, 85, 1704−1714